ISSN 1674-1056
http://cpb.iphy.ac.cn
http://iopscience.iop.org/cpb
中国物理 B
Chinese Physics
中国物理 Chinese Physics B

Analysis of meniscus beneath metastable droplets and wetting transition on micro/nano textured surfaces

Yanjie Li(李艳杰), Xiangqin Li(李香琴), Tianqing Liu(刘天庆), Weiguo Song(宋伟国)

Citation: Chin. Phys. B . 2018, 27(8): 086801. **doi:** 10.1088/1674-1056/27/8/086801

Journal homepage: http://cpb.iphy.ac.cn; http://iopscience.iop.org/cpb

What follows is a list of articles you may be interested in

The influence of surface effects on Frederiks transition in nematic liquid crystal doped with ferroelectric nanoparticles

Erfan Kadivar, Mojtaba Farrokhbin

Chin. Phys. B . 2018, 27(4): 046801. **doi:** 10.1088/1674-1056/27/4/046801

Effects of grinding-induced grain boundary and interfaces on electrical transportation and structure phase transition in ZnSe under high pressure

Jie Yang(杨洁), Pei Wang(汪沛), Guo-Zhao Zhang(张国召), Xiao-Xue Zhou(周晓雪), Jing Li(李静), Cai-Long Liu(刘才龙)

Chin. Phys. B . 2016, 25(6): 066802. **doi:** 10.1088/1674-1056/25/6/066802

Theoretical analysis of droplet transition from Cassie to Wenzel state

Liu Tian-Qing, Li Yan-Jie, Li Xiang-Qin, Sun Wei

Chin. Phys. B . 2015, 24(11): 116801. **doi:** 10.1088/1674-1056/24/11/116801

Contact angle hysteresis in electrowetting on dielectric

Zhao Rui, Liu Qi-Chao, Wang Ping, Liang Zhong-Cheng

Chin. Phys. B . 2015, 24(8): 086801. **doi:** 10.1088/1674-1056/24/8/086801

Fabrication of pillar-array superhydrophobic silicon surface and thermodynamic analysis on the wetting state transition

Liu Si-Si, Zhang Chao-Hui, Zhang Han-Bing, Zhou Jie, He Jian-Guo, Yin Heng-Yang

Chin. Phys. B . 2013, 22(10): 106801. **doi:** 10.1088/1674-1056/22/10/106801

Analysis of meniscus beneath metastable droplets and wetting transition on micro/nano textured surfaces*

Yanjie Li(李艳杰)[2], Xiangqin Li(李香琴)[1], Tianqing Liu(刘天庆)[1,†], and Weiguo Song(宋伟国)[2,‡]

[1] *School of Chemical Engineering, Dalian University of Technology, Dalian* 116024, *China*
[2] *School of Pharmacy, Weifang Medical University, Weifang* 261053, *China*

(Received 25 December 2017; revised manuscript received 22 May 2018; published online 25 July 2018)

The expressions of interface free energy (IFE) of composite droplets with meniscal liquid–air interface in metastable state on micro/nano textured surfaces were formulated. Then the parameters to describe the meniscus were determined based on the principle of minimum IFE. Furthermore, the IFE barriers and the necessary and sufficient conditions of drop wetting transition from Cassie to Wenzel were analyzed and the corresponding criteria were formulated. The results show that the liquid–air interface below a composite droplet is flat when the post pitches are relatively small, but in a shape of curved meniscus when the piteches are comparatively large and the curvature depends on structural parameters. The angle between meniscus and pillar wall is just equal to the supplementary angle of intrinsic contact angle of post material. The calculations also illustrate that Cassie droplets will transform to Wenzel state when post pitch is large enough or when drop volume is sufficiently small. The opposite transition from Wenzel to Cassie state, however, is unable to take place spontaneously because the energy barrier is always positive. Finally, the calculation results of this model are well consistent with the experimental observations in literatures for the wetting transition of droplets from Cassie to Wenzel state.

Keywords: interface free energy, droplet, wetting, transition, energy barrier

PACS: 68.08.–p, 68.08.Bc **DOI:** 10.1088/1674-1056/27/8/086801

1. Introduction

Droplets on micro/nano textured surfaces may appear in the states of Cassie (with flat liquid–air interface beneath), Wenzel, or composite (with curved liquid–air interface) as shown in Fig. 1. Drops show large contact angles and small contact angle hysteresis, i.e., suerhydrophobic properties, only when they exist in Cassie or in composite state. However, when droplets appear in Wenzel state, contact angle hysteresis is substantial, and the surface loses its superhydrophobicity. Therefore, the wetting states of droplets and whether they transform from Cassie to Wenzel state (C–W) on rough surfaces are the key research contents of superhydrophobic materials.

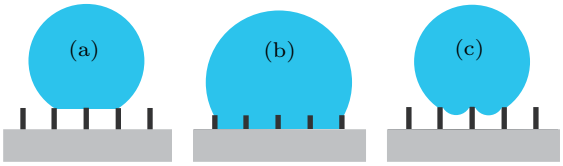


Fig. 1. Schematics of Cassie (A) with flat liquid–air interface beneath, Wenzel (B), and composite droplet (C) with curved liquid–air interface on a textured surface.

Most researchers considered the shape of liquid–air interface beneath a composite droplet as a plane or a straight line (Fig. 1(a)).[1–4] However, this model does not accord with wetting characters of liquid on pillar surfaces, which usually shows a curved liquid–air interface or meniscus. Also the model cannot explain why the height of posts influences the C–W transition.[5–9] In fact, the bending liquid–air interface below a composite droplet has been proved by several experiments.[9–12] And more and more models accepted the meniscus[5–7,13–18] although most of them were two dimensional models with a piece of arc to show the liquid–air interface between two pillars (Fig. 1(c)).[5,6,13,17] There are several methods to determine the curvature radius of the arc. When a droplet is not acted by external forces, it is generally considered that the angle between this arc and pillar wall is equal to the supplementary angle of intrinsic contact angle.[5,18] On the other hand, the curvature radius of this arc might be taken as the same as the spherical radius of droplet.[5,7,19] Meanwhile, the curvature of the arc increases with external forces, such as hydraulic pressure and static electricity.[11–15]

The condensed drop shapes on nanostructures observed by Rykaczewski[10] showed that the liquid–air interface between posts with small pitches indeed appeared in arc. Whereas the experiment by Ensikat *et al.*[20] indicated that the liquid–air interface between posts with large pitches appeared in plane without obvious bending, and curvature only existed near pillar walls. Meanwhile, a clear meniscus would appear when a droplet was acted by external pressure or electric wetting force.[11–15] Therefore, the shape of bending liquid–air interface is relevant to not only structural parameters but also the action of external forces. When a droplet is not acted by

*Project supported by the National Natural Science Foundation of China (Grant No. 21676041).
†Corresponding author. E-mail: liutq@dlut.edu.cn
‡Corresponding author. E-mail: songwg@139.com
© 2018 Chinese Physical Society and IOP Publishing Ltd

external pressure, its bottom liquid–air interface profile is not necessarily always an arc.

Minimizing of interface free energy (IFE) of droplets is often used to determine its wetting state,[1,3,21–25] including equilibrium contact angle etc. Multi-peak values[2,22] may exist for the IFE of droplets on textured surfaces. Locally minimum and globally minimal IFE are corresponding to the metastable and the most stable drops, respectively. A metastable droplet is unable to transform to the most stable state spontaneously because there is an energy barrier to overcome. Consequently, Cassie drops or composite droplets can exist stably although they are not in the lowest energy state.[27] Only when certain pressure or electric wetting force[11–15,17] acts on a metastable drop, it may transit to wetted state.

Droplet IFE is relevant to the shape of liquid–air interface, but almost all IFE calculations did not involve the curvature of the interface.[1–3,21–25] Only very few two dimensional models[5] were based on the bending interface without three dimension calculations so far. Additionally, only contact angles were generally calculated by means of IFE minimum[2,24] while the parameters describing meniscus were not solved until today.

On the other hand, the mechanism of droplet C–W transition has been investigated heavily,[3–9,11–15,17–19,22,25–41] which is classified into two types, external force driving and spontaneous evolution. External forces include static pressure or hydraulics pressure,[11,12,15,17,18,40] impact force of droplet landing from high place[38,42] or deceleration force,[41] and static electricity wetting force.[13,14,34] The effect of gravity could be ignored for a droplet if its scale is less than the capillary length.[9] The so-called spontaneous transition means the collapse of a Cassie droplet on structural surface not by external force, but only by the interaction between the droplet and the textured surface. For example, an evaporating droplet on a rough surface will convert from composite state to Wenzel state spontaneously when its volume decreases to a critical value.[7,9,17,35,36] Until today however, this mechanism of the spontaneous transition is still not clear. There are a few conflicted interpretations, including the Laplace pressure inside droplets as the transition driving force,[7,15,37,38] the external force overcoming the Laplace pressure,[17] the gravity of droplets as driving force[4,6,39] etc.

It is generally considered that the C–W transition needs to overcome a energy barrier,[3,5,19,25,27,30–32,43,44] and the barrier of drop evolution from Wenzel to Cassie state (W–C) is always greater than the one of C–W transition.[28,31] Therefore, W–C alteration is more difficult and the two transition processes are considered irreversible.[28] Moreover, contact angles were usually regarded as constants when calculating energy barriers,[30,32,43,44] which would lead to energy barriers always positive.[27,43,44] For instance, Zheng *et al.*[32] derived that W–C barrier was adhesion work while C–W barrier was wetting work. The forever positive of C–W barrier means the transition can not be completed spontaneously unless the action of an external force. But the truth is that the C–W transition is able to be accomplished spontaneously for small droplets sitting on posts with relatively large pitches. Consequently, C–W energy barriers might disappear or become negative[25] under certain conditions. In a word, more reasonable calculation of C–W and W–C energy barriers is still absent.

A three-dimensional (3D) model of the meniscus beneath a sessile droplet on textured surface was founded in this study. The droplet IFE was formulated with multi variables, and the parameters depicting the meniscus of a composite droplet in metastable state were determined based on the principle of IFE minimizing. Finally the energy barriers of C–W and W–C transition were calculated and the necessary and sufficient conditions of C–W transition were figured out.

2. Physical model

The metastable and most stable states of a sessile droplet are corresponding to its IFE locally and globally minimal respectively. In many cases although the IFE of a metastable composite drop with its IFE locally minimal is greater than that when it is in Wenzel state, the composite droplet still does not transit to Wenzel state because of the existing of energy barrier. Therefore, sessile drops usually appear in composite state suspending on pillars. The shape and the minimum IFE of a composite droplet are analyzed below. As shown in Fig. 2, a small composite drop is supposed to be a segment since its gravity is ignored. The whole volume of droplet is divided into two parts, segment volume above posts $V_{\rm up}$ and the volume into structures $V_{\rm in}$. The liquid–air interface beneath drop may be curved. The local liquid–air interface around a pillar is formed by an arc rotating once on the pillar. The radius of the arc is R, downwards bending depth of meniscus is h_x, and the angle between arc and pillar wall is ϕ. A straight line with length of l links the two arcs on two adjacent posts. Besides, the diameter, pitch, and the height of pillars are d, p, and H respectively. Contact angle and base radius of droplet are θ and $r_{\rm s}$ respectively. And x means infiltration length on posts. Thus for pillars in square array, the meniscus among four pillars is made of the curved surfaces on pillar side walls and the middle flat surface.

The above mentioned multi variables, θ, $r_{\rm s}$, x, R, ϕ, h_x, and l, are used to describe the meniscus of a metastable droplet on textured surfaces. These parameters can be determined based on the method of drop IFE minimum. In order to calculate the IFE, the expressions of meniscus area and volume into textures beneath a droplet have to be established firstly.

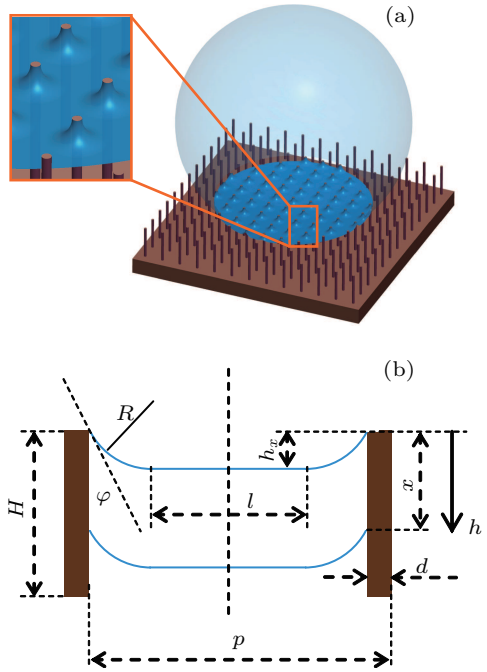


Fig. 2. (color online) Schematics of liquid–air interface beneath composite droplet on textured surface. (a) 3D liquid–air interface; (b) curves of liquid–air interface between two adjacent pillars and related parameters.

3. Mathematical model

3.1. Independent variables used to describe the mensicus

We used the seven varables to dispict the mensicus beneath a droplet on textured surfaces, i.e., θ, r_s, x, R, ϕ, h_x, and l, as shown in Fig. 2 and stated in the physical model. But only four variables among them are independent since there are two following relations which can be easily found for the arc on a pillar wall shown in Fig. 2:

$$h_x = R(1-\sin\varphi), \tag{1}$$

$$l = p - d - 2R\cos\varphi. \tag{2}$$

Besides, x can be expressed with variables θ, r_s, R, and φ, as shown in the latter Eq. (10). Therefore, the four variables, θ, r_s, R, and φ are selected as independent ones in this model. And they will be determined based on the IFE minimum of a droplet as shown in the latter sections of this model.

3.2. Liquid–air interfacial area around a post

Based on the above physical model, the liquid–air interface area formed by the rotation of the arc on a post is:

$$\begin{aligned} A_1 &= \int_0^{\pi/2-\varphi} 2\pi\left(\frac{d}{2}+R\cos\varphi - R\sin\alpha\right)R\mathrm{d}\alpha \\ &= 2\pi R^2\left[\left(\frac{d}{2R}+\cos\varphi\right)\left(\frac{\pi}{2}-\varphi\right)+\sin\varphi-1\right]. \end{aligned} \tag{3}$$

3.3. Meniscus area beneath droplet

The meniscus area beneath a droplet on cylindrical posts in square array is expressed by

$$\begin{aligned} A_{\mathrm{blg}} &= \pi r_s^2\frac{p^2-\pi(d/2+R\cos\varphi)^2+A_1}{p^2} \\ &= \pi r_s^2\left\{1-\frac{\pi}{p^2}\left(\frac{d}{2}+R\cos\varphi\right)^2\right. \\ &\quad \left.+\frac{2\pi R^2}{p^2}\left[\left(\frac{d}{2R}+\cos\varphi\right)\left(\frac{\pi}{2}-\varphi\right)+\sin\varphi-1\right]\right\}. \end{aligned} \tag{4}$$

3.4. Volume between pillar wall and surrounded liquid–air interface

The air volume between a pillar wall and the surrounded liquid–air interface is the integral:

$$\begin{aligned} V_1 &= \int_0^{h_x}\pi\left\{\left[R\cos\varphi+\frac{d}{2}-\sqrt{(R^2-(R-h_x+z)^2)}\right]^2\right. \\ &\quad \left.-\frac{d^2}{4}\right\}\mathrm{d}z, \end{aligned} \tag{5}$$

which becomes this equation after simplification:

$$\begin{aligned} V_1 &= \pi R^2(1-\sin\varphi)\left[2R+d\cos\varphi-\frac{R(1-\sin\varphi)^2}{3}\right] \\ &\quad +\pi R^2\left[\frac{d}{2}\sin\varphi\cos\varphi-\left(\frac{\pi}{2}-\varphi\right)\left(\frac{d}{2}+\cos\varphi R\right)\right]. \end{aligned} \tag{6}$$

3.5. Volume into textures beneath a droplet

This volume is expressed as

$$V_{\mathrm{in}} = \pi r_s^2\left[(1-f)x+(1-f)h_x-\frac{V_1}{p^2}\right], \tag{7}$$

where f is the solid area fraction of a textured surface. After V_1 is substituted, equation (7) becomes

$$\begin{aligned} V_{\mathrm{in}} &= \pi r_s^2\left\{(1-f)\left[x+R(1-\sin\varphi)\right]\right. \\ &\quad -\frac{\pi R^2(1-\sin\varphi)}{p^2}\left[2R+d\cos\varphi-\frac{R(1-\sin\varphi)^2}{3}\right] \\ &\quad \left.-\frac{\pi R^2}{p^2}\left[\frac{d}{2}\sin\varphi\cos\varphi-\left(\frac{\pi}{2}-\varphi\right)\left(\frac{d}{2}+\cos\varphi R\right)\right]\right\}. \end{aligned} \tag{8}$$

And the whole drop volume is

$$V = V_{\mathrm{up}}+V_{\mathrm{in}} = \frac{1}{3}\pi r_s^3\frac{(2-3\cos\theta+\cos^3\theta)}{\sin^3\theta}+V_{\mathrm{in}}, \tag{9}$$

where the contact angle θ is the apparent one of the segment with volume V_{up}, i.e. the one considered the drop volume into pillar structures.

From the above two equations x can be expressed with the four independent variables:

$$x = \frac{1}{1-f}\left\{\frac{V}{\pi r_s^2}-\frac{1}{3}r_s\frac{(2-3\cos\theta+\cos^3\theta)}{\sin^3\theta}\right.$$

$$-R(1-\sin\varphi)(1-f) + \frac{\pi R^2(1-\sin\varphi)}{p^2}\left[2R+d\cos\varphi-\frac{R(1-\sin\varphi)^2}{3}\right] + \frac{\pi R^2}{p^2}\left[\frac{d}{2}\sin\varphi\cos\varphi-\left(\frac{\pi}{2}-\varphi\right)\left(\frac{d}{2}+\cos\varphi R\right)\right]\Bigg\}. \quad (10)$$

3.6. IFE and total liquid–air interface area of a droplet

For a droplet on textured surface with selected projection area A_{total}, the IFE includes liquid–air, solid–air, and solid–liquid interfacial energy[25]

$$\begin{aligned} E &= (A_{\text{d}}+A_{\text{blg}})\sigma_{\text{LG}}+(rA_{\text{total}}-A_{\text{bsl}})\sigma_{\text{SG}}+A_{\text{bsl}}\sigma_{\text{SL}} \\ &= (A_{\text{d}}+A_{\text{blg}})\sigma_{\text{LG}}-A_{\text{bsl}}\cos\theta_{\text{I}}\sigma_{\text{LG}}+rA_{\text{total}}\sigma_{\text{SG}}, \end{aligned} \quad (11)$$

where r is Wenzel rough factor; A_{d} and A_{bsl} are the droplet upper liquid–air area and the solid-liquid contact area beneath the drop respectively; σ_{LG}, σ_{SG}, and σ_{SL} are liquid–gas, solid–gas, and solid–liquid interfacial energy; θ_{I} is intrinsic contact angle. The expressions of A_{d} and A_{bsl} respectively are

$$A_{\text{d}} = \frac{2\pi r_{\text{s}}^2}{1+\cos\theta}, \quad (12)$$

$$A_{\text{bsl}} = \pi r_{\text{s}}^2\left[f+(r-1)\frac{x}{H}\right]. \quad (13)$$

After substituting all areas into Eq. (11), the IFE becomes

$$\begin{aligned} E &= \pi r_{\text{s}}^2\sigma_{\text{LG}}\left\{\frac{2}{1+\cos\theta}+1-\frac{\pi}{p^2}\left(\frac{d}{2}+R\cos\varphi\right)^2\right. \\ &\quad +\frac{2\pi R^2}{p^2}\left[\left(\frac{d}{2R}+\cos\varphi\right)\left(\frac{\pi}{2}-\varphi\right)+\sin\varphi-1\right] \\ &\quad \left.-\left[f+(r-1)\frac{x}{H}\right]\cos\theta_{\text{I}}\right\} \\ &\quad +rA_{\text{total}}\sigma_{\text{SG}}. \end{aligned} \quad (14)$$

The total liquid–air area of a droplet is

$$A = A_{\text{d}}+A_{\text{blg}}. \quad (15)$$

Besides, the IFE and total liquid–air area of a Cassie droplet are

$$E_{\text{C}} = \pi r_{\text{sC}}^2\sigma_{\text{LG}}\left(\frac{2}{1+\cos\theta_{\text{EC}}}-\cos\theta_{\text{EC}}\right)+rA_{\text{total}}\sigma_{\text{SG}}, \quad (16)$$

$$A_{\text{C}} = \pi r_{\text{sC}}^2\left(\frac{2}{1+\cos\theta_{\text{EC}}}+1-f\right), \quad (17)$$

in which θ_{EC} and r_{sC} means the equilibrium contact angle and base radius of a Cassie drop, respectively

$$\cos\theta_{\text{EC}} = f\cos\theta_{\text{I}}+f-1, \quad (18)$$

$$r_{\text{sC}} = \left[\frac{3V}{\pi(1-\cos\theta_{\text{EC}})^2(2+\cos\theta_{\text{EC}})}\right]^{1/3}\sin\theta_{\text{EC}}. \quad (19)$$

3.7. Determination of minimum IFE and shape parameters of droplets

The IFE expression of a drop with four independent variables, θ, r_{s}, R, and φ, can be obtained by substituting Eq. (10) into Eq. (14). Then, these four parameters of droplet shape can be determined based on the IFE minimizing, i.e., the following equations of partial derivatives

$$\frac{\partial E}{\partial\theta} = 0, \quad (20)$$

$$\frac{\partial E}{\partial r_{\text{s}}} = 0, \quad (21)$$

$$\frac{\partial E}{\partial R} = 0, \quad (22)$$

$$\frac{\partial E}{\partial\varphi} = 0, \quad (23)$$

which were solved by using the function of "fmincon" in Matlab. The corresponding constraint conditions include: $0\le\theta\le\pi$, $0\le r_{\text{s}}$, $0\le R\le(p-d)/(2\cos\varphi)$, $0\le\varphi\le\pi/2$, and $0\le x\le H$. And the calculation program is in the supplementary material.

If the calculation results show $x=H$, it means that the drop has completely infiltrated posts. In this case, composite metastable droplet does not exist, i.e. it has changed to Wenzel state, which is in the unique minimum IFE. The IFE of a Wenzel droplet is expressed by

$$E_{\text{W}} = \pi r_{\text{sW}}^2\sigma_{\text{LG}}\left[\frac{2}{1+\cos\theta_{\text{EW}}}-\cos\theta_{\text{EW}}\right]+rA_{\text{total}}\sigma_{\text{SG}}, \quad (24)$$

where θ_{EW} and r_{sW} are the equilibrium contact angle and base radius respectively:

$$\theta_{\text{EW}} = r\cos\theta_{\text{I}}, \quad (25)$$

$$r_{\text{sW}} = \left[\frac{3V}{\pi(1-\cos\theta_{\text{EW}})^2(2+\cos\theta_{\text{EW}})}\right]^{1/3}\sin\theta_{\text{EW}}. \quad (26)$$

3.8. Energy barrier of C–W and W–C transition

Energy barriers usually exist for C–W and W–C transition, which are defined as follows.

The energy barrier of C–W transition, E_{bC}, is defined as the IFE difference between a special composite drop with its base radius equal to that of Cassie drop when its infiltration length x equals to pillar height H and the Cassie droplet, namely

$$E_{\text{bC}} = E_1|_{x=H}-E_{\text{C}}, \quad (27)$$

where $E_1|_{x=H}$ is expressed by

$$E_1|_{x=H} = \pi r_{\text{sC}}^2\sigma_{\text{LG}}\left[\frac{2}{1+\cos\theta_{\text{S1}}}-\cos\theta_{\text{ES}}\right]+rA_{\text{total}}\sigma_{\text{SG}}, \quad (28)$$

in which θ_{ES} is the equilibrium contact angle of the special composite drop determined by this formular[25]

$$\cos\theta_{\text{ES}} = (f+r-1)\cos\theta_{\text{I}}+f-1. \quad (29)$$

And θ_{S1} is its apparent contact angle, which can be found from the following equation

$$V = V_{up} + V_{in} = \frac{1}{3}\pi r_{sC}^3 \frac{(2-3\cos\theta_{S1}+\cos^3\theta_{S1})}{\sin^3\theta_{S1}} + \pi r_{sC}^2(1-f)H. \quad (30)$$

Then the E_{bc} can be expressed as

$$E_{bc1} = \pi r_{sC}^2 \sigma_{LG}\left[\frac{2}{1+\cos\theta_{S1}} - \frac{2}{f(1+\cos\theta_I)} - (r-1)\cos\theta_I\right]. \quad (31)$$

On the other hand, the energy barrier of W–C transition, E_{bW}, is defined as the IFE difference between a special composite drop with its base radius equal to that of Wenzel drop when its infiltration length x equals to pillar height H and the Wenzel droplet, namely:

$$E_{bW} = E_2|_{x=H} - E_W, \quad (32)$$

where $E_2|_{x=H}$ is expressed by

$$E_2|_{x=H} = \pi r_{sW}^2 \sigma_{LG}\left[\frac{2}{1+\cos\theta_{S2}} - \cos\theta_{ES}\right] + rA_{total}\sigma_{SG}, \quad (33)$$

in which θ_{S2} is the apparent contact angle of the special composite drop and it can be found from this equation

$$V = V_{up} + V_{in} = \frac{1}{3}\pi r_{sW}^3 \frac{(2-3\cos\theta_{S2}+\cos^3\theta_{S2})}{\sin^3\theta_{S2}} + \pi r_{sW}^2(1-f)H. \quad (34)$$

The textured surfaces with cylindrical micro/nano-posts were considered in the calculation. And the solid area fraction and Wenzel rough factor for this type of posts are:

$$f = \pi(d/p)^2/4, \quad (35)$$

$$r = 1 + \pi dH/p^2. \quad (36)$$

4. Results and discussion

4.1. Comparison of locally minimal IFE of composite droplets with IFE of Cassie drops

Figure 3 shows the IFE difference and liquid–air area difference between Cassie droplet and composite drop with local IFE minimum. It can be seen that the IFE difference is negative when pillar pitch is small, which means that the IFE of Cassie drop is lower than that of the composite droplet with curved liquid–air interface underneath. Correspondingly, the liquid–air area of Cassie droplet is also smaller than that of composite drop in this case. As pillar pitch increases, however, both the difference of IFE and the difference of liquid–air area between the two types of droplets become positive, which indicates that the IFE of the composite drop with meniscus starts to be lower than that of Cassie droplet so that it exists more stably. The liquid–air area of the two types of droplets considered here is the total liquid–air area, including the upper area of segment. Although the curved meniscus area beneath a composite droplet is larger than that of Cassie drop, its liquid–air area of segment part may be much less than that of Cassie drop. Therefore, the difference of liquid–air area may become positive.

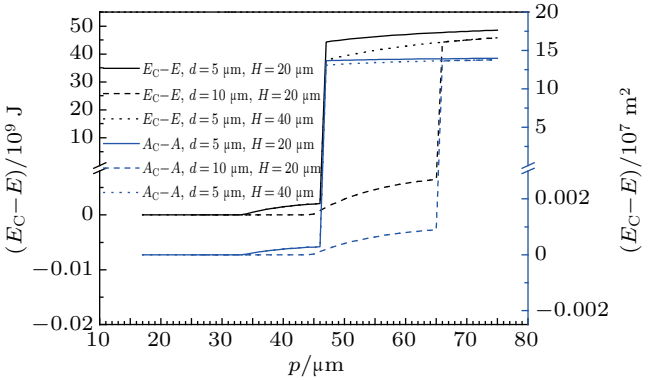


Fig. 3. (color online) Comparison of IFE and liquid–air area between Cassie and composite droplet with IFE minimum on textured surfaces. $V = 2$ μL, $\theta = 110°$.

Besides, it is also clear from Fig. 3 that on the two textured surfaces with post diameters of 5 μm and 10 μm, both the IFE difference and the liquid–air area rise abruptly when the pitch of pillars is 47 μm and 66 μm respectively for the two surfaces. This is because the transition of the droplet from the composite state to Wenzel takes place, after which metastable composite drops will no longer exist while only Wenzel droplets with global IFE minimum appear on the surfaces. Furthermore, it is also clear that the pillar height does not have much influence either on the IFE difference and liquid–air area difference of the two types of droplets or on the disappearing of the metastable drops. But the effects of the post diameter are obvious. The larger the diameter, the greater the IFE difference, and the larger the pillar pitch needed for C–W transition.

Above results indicate that the liquid–air interface beneath a composite droplet is a flat one, i.e., a Cassie drop, when pillar pitch is small. But it will become curved when pillar pitch is large.

This model supposed that there is no force acting on the droplet and the interface free energy is the lowest. However, the droplet bottom is always in meniscus when there is driving force acting on the droplet, which is called interface free energy gradient[45] or Laplace pressure in some literatures.[7,15,37,38] But in that case, droplet is not free and the interface free energy is not in the lowest state. Consequently, there is some error between the calculation results of this study and the actual condition.

4.2. Comparison of locally minimal IFE of composite droplets with IFE of Wenzel drops

Figure 4 shows the IFE difference between composite droplet with local IFE minimum and Wenzel drop on different textured surfaces. It is clear from the figure that the IFE of composite droplet is lower than that of Wenzel drop when pillar pitch is small, which means that Wenzel drop is in metastable state while composite droplet is in the most stable state with global IFE lowest. When pillar pitch becomes large, however, the situation turns to be opposite. That is, the IFE of composite droplet is higher than that of Wenzel drop so that composite droplet is in metastable state while Wenzel drop is in the most stable state. If pillar pitch increases further, local IFE minimum will disappear, i.e. metastable composite droplets no longer exist but Wenzel drops live since there is only global IFE minimum in this case. Therefore, the vanishing of local IFE minimum of composite drop is one of the necessary conditions of C–W transition.

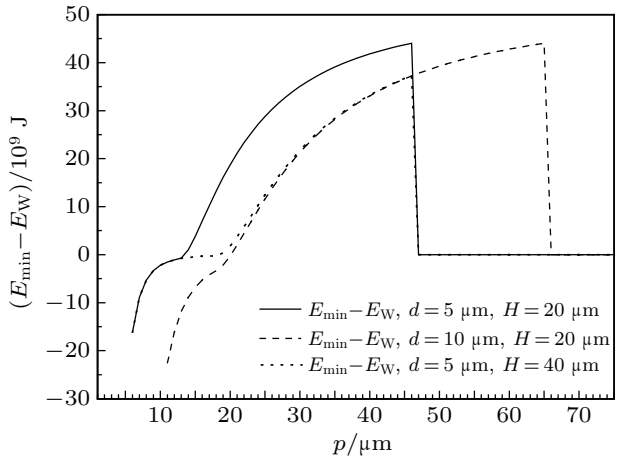


Fig. 4. Comparison of IFE between Wenzel and composite droplet with IFE minimum, E_{min} on textured surfaces. $V=2$ μL, $\theta_I=110°$

4.3. Parameters of composite droplets with IFE minimum

Figure 5 shows the multi parameters of composite droplet shape in the state of locally lowest IFE on different textured surfaces. It can be seen that the curvature radius R of the liquid–air interface below the drop is zero when pillar pitches are small (Fig. 5(a)), i.e. the liquid–air interface is not curved. In this case a straight lined liquid–air interface directly link the two adjacent pillar walls, i.e., $l=p-d$. That is, the liquid–air interface beneath the droplet is a flat one, as a Cassie drop. When the pitches further increase, however, R starts to increase continuously while l still exists. Namely, the liquid–air interface below a composite droplet in this case contains both curved and flat parts. Finally, when the pitches further enlarge, the composite drop will change to Wenzel state with meniscus distinguishing and R becoming zero again.

The above results show that the meniscus below a composite droplet with minimum IFE includes not only curved part but also a flat one, which is a little different from the model of one complete arc between two posts accepted in several literatures.[5,6,13,17] It should be declared that our model is only valid for droplets without any external force acted and in the locally lowest IFE. When a composite drop is acted by pressure etc, the meniscus beneath it will become a absolute arc, but its IFE is not in minimum state in this case. Therefore the shape parameters of a composite droplet cannot be determined by the method of IFE minimum in this latter situation.

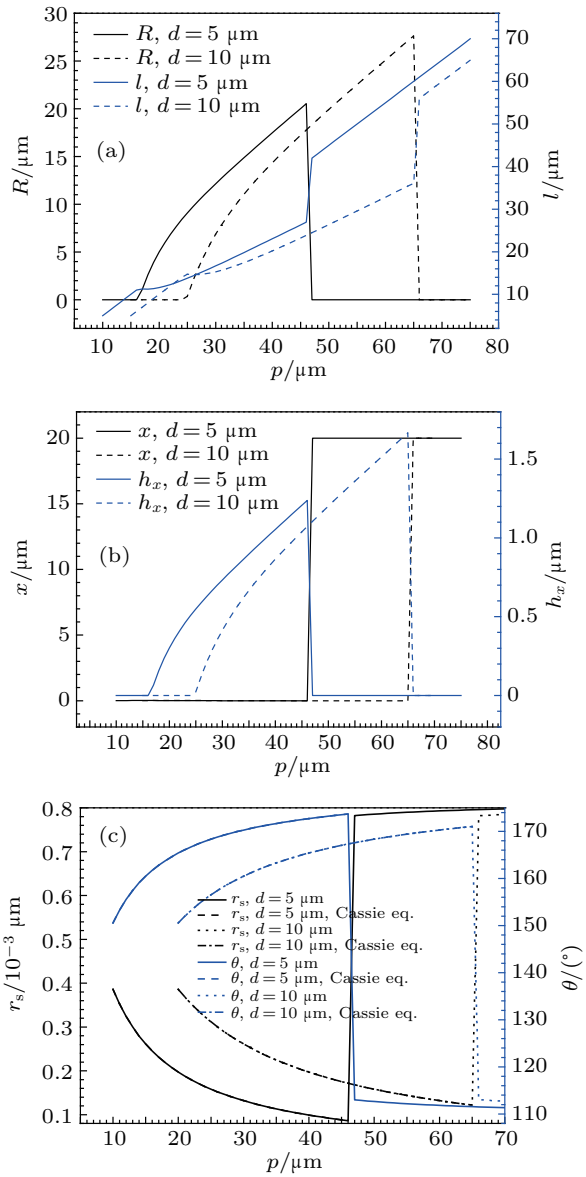


Fig. 5. (color online) Parameters of composite droplet with IFE minimum. (a) R and l change with p; (b) x and h_x change with p; (C) r_s andθ change with p. $V=2$ μL, $\theta_I=110°$, $H=20$ μm.

The calculation for composite droplets with IFE minimum also indicates that the angle φ between liquid–air interface and pillar wall constantly equals to $\pi-\theta_I$ (data not shown). This result illustrates that the wetting state of droplet on pillar side walls accords to the intrinsic contact angle, which is the same as that supposed in literatures.[5,18] Additionally, it is clear from Figs. 5(a) and 5(b) that the chang-

ing regularity of h_x is completely similar to that of R, which is already shown in Eq. (1). Besides, it can also be seen from Fig. 5(b) that infiltration length x on pillar walls beneath droplet is almost zero when pillar pitch is small. But x will quickly equals to pillar height H, which means that the posts below drop have been completely infiltrated. Therefore, $x = H$ is another necessary condition of C–W transition. Moreover, it can be found from both Figs. 5(a) and 5(b) that pillar diameter influences both the curvature of liquid–air interface below droplet and C–W transition obviously. The greater the pillar diameter, the larger the maximum R and h_x, and the larger the p needed to complete C–W transition.

Although the liquid–air interface beneath a composite droplet on textured surfaces may be curved, which is different from the plane interface below a Cassie drop, contact angles and base radius of the composite droplet are almost the same as those of Cassie drop, as shown in Fig. 5(c). This result indicates that the meniscus below composite droplet influences the shape of upper drop on posts weakly. In fact, the most part of a droplet volume locates outside of micro/nanostructures while only very small ratio is inside. Therefore, contact angle and base radius of metastable composite droplets can be calculated with Cassie-Baxter equation.

Even though the meniscus of metastable drop does not affect contact angle obviously, it indeed influences the C–W transition especially in the case of short posts which make the meniscus below droplet touch the structural substrate easily.[6,7,25] But the effect of pillar height on C–W transition can not be explained with the flat liquid–air interface beneath Cassie drops.[5–8,25]

The IFE of sessile droplets on textured surfaces was analyzed in this study, and the curvature of meniscus below these drops is small. For instance, the h_x in Fig. 5(b) is only a few micrometers. Relatively large droplets deposited on surfaces are consistent with this situation. On the other hand, the measured h_x could be as deep as 4 μm–23 μm[9,11,12] when droplets were acted by external force[11,12,15,17,18] or electric wetting force,[13,14,34] or during the evaporation of drops.[7,9,17,35,36] And the measured h_x is obviously larger than the calculated value. This demonstrates that droplets are not in the metastable state with local IFE minimum when there is external force or when evaporation takes place. In fact extra energy will add to drops in this case, which leads to the curvature of meniscus increasing. Therefore, the bending liquid–air interface should be determined according to the real free energy of droplets in these cases, but not based on the minimum IFE of this model.

In this study, we didn't consider the force condition of the droplet. Consequently, the calculation result that the contact angle keeps constant is obtained when droplet is in the lowest free energy condition. However, when there is force acting on the droplet the contact angle between micropillar and droplet is constantly changing. In other word, in the actual conditions of C–W transition process contact angle changes from small to large.

4.4. Energy barriers of C–W and W–C transition

The energy barriers of C–W and W–C transitions on different textured surfaces are shown in Fig. 6. It can be seen that the C–W barriers become negative (see Fig. 6(b)) when pillar pitch is large enough. The negative barrier means that the IFE of Cassie droplet is higher than that of any composite drop with different infiltration lengths on pillar walls. Namely, the IFE of Cassie droplet is the greatest globally. Besides, the negative C–W barrier also means that the C–W transition may take place spontaneously because the transformation process is from higher energy to lower energy. On the other hand, the energy barrier of W–C is always positive (Fig. 6(a)), i.e. the transition is unable to happen spontaneously. Furthermore, it is also clear from Fig. 6(b) that the larger the pillar diameter, the greater the pitch needed to make the C–W barrier become negative. But the influence of pillar height on C–W transition is very weak. For instance, the needed pitch for the transition is the same around 46 μm–47 μm when pillar height is 20 μm and 40 μm respectively. The only difference between the two pillar heights is that the energy barrier with $H = 40$ μm decreases faster with pitch enlargement (as shown in Fig. 6(b)).

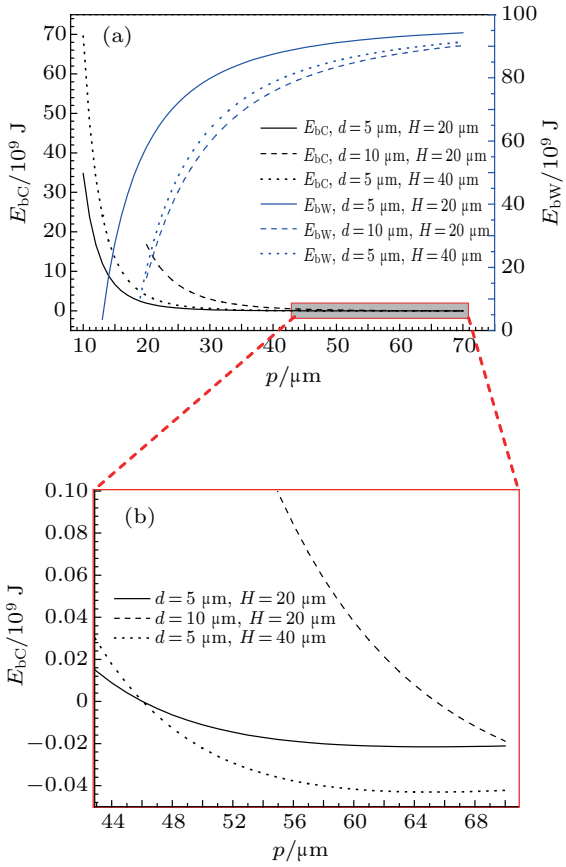


Fig. 6. (color online) Energy barriers of C–W and W–C transition change with pillar pitches. $V = 2$ μL, $\theta_l = 110°$. Panel (b) is the local amplification of panel (a).

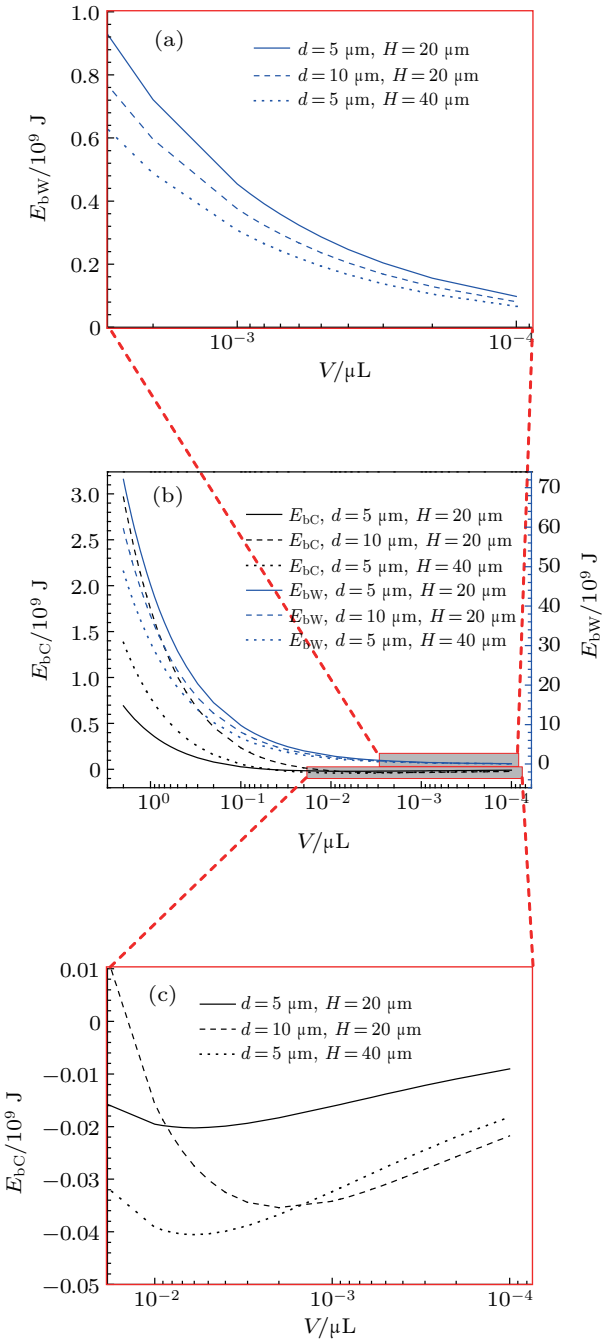


Fig. 7. (color online) Energy barriers of C–W and W–C transition change with drop volumes. $p - d = 20$ μm, $\theta_I = 110°$. Panels (a) and (c) are the local amplifications of panel (b).

The effect of drop volume on the energy barriers of C–W and W–C transition is shown in Fig. 7. It is clear that the two types of barriers all decline with the decrease of V. And the C–W barrier can become negative if V is small enough (Fig. 7(c)). In contrast, the W–C barrier is always positive (Fig. 7(a)). Consequently, C–W transition may be completed spontaneously under the conditions that pillar pitch is sufficiently large (Fig. 6(b)) or drop volume is small enough (Fig. 7(c)), which accords well with experiments.[7,9,25,35,36] But W–C transition is unable to take place spontaneously no matter under what conditions. That is, W–C transition may be completed only by the excitation of external energy, such as vibration.[21,46]

By comparing the two necessary conditions of C–W transition, the above C–W energy barrier being zero and the early $x = H$ condition, it can be seen that both are completely consistent. Therefore, both of them can be used to calculate the C–W transition. It can be said that the basic reason for C–W transition of a metastable drop on textured surface is the disappearing of its local IFE minimum value, or the vanishing of C–W energy barrier. The C–W transition may be inhibited by proper control of the patterns of structures and surface chemical characters, such as by increasing the roughness of pillar sides,[47,48] manufacturing two-tier structures,[17,43,49,50] and raising the intrinsic contact angle of surface materials.[49] The mechanism proposed here for C–W transition can be used to explain and predict the phenomenon of wetting state transformation during droplet evaporation.

It is necessary to further mention that the droplet apparent contact angles were supposed to be unchanging for the calculation of C–W transition energy barrier in almost all published models.[25,30,32,43] We considered, however, this assumption may result in obvious errors when droplet is small or when the droplet volume entering into structures can not be ignored. And the influence of drop volume inside textures on C–W energy barrier was considered in this study as shown from Eqs. (27)–(33). Namely, the drop volume above textures decreases, and the apparent contact angle also declines during C–W transition under the condition of base radius unchanging, which was already proved by the experimental observations[36] during meniscus declining. Therefore, the formulas proposed in this model can describe the real case more closely. In the matter of fact, the C–W energy barrier will become wetting work[32,38,43] and always positive if the drop volume entering textures is not considered or the drop apparent contact angle is regarded as constant. If so, the C–W transition of droplets on any textured surfaces would be unable to be completed spontaneously. But the truth is Cassie droplets can spontaneously transform into Wenzel state[7,9,17,25,35,36] when pillar pitch is large enough or when drop volume is sufficiently small. Consequently, the change of apparent contact angle or the drop volume entering structures must be considered for the calculation of C–W energy barriers.

4.5. Necessary and sufficient conditions of C–W transition

The work needed to drive the three phase contact line (TPCL) moving along pillar walls beneath droplets was also regarded as a part of C–W energy barrier in the calculations of Bormashenko *et al.*'s.[44] But we consider that energy barrier is a kind of state function since IFE is a state function and the enerby barrier here is the IFE difference between two droplets with different wetting states, not relevant to the path of droplet TPCL moving along pillar walls. This is just similar to the

energy barrier between valley and peak. The barrier in this case only depends on the potential difference between the two locations, but not relevant to the pathways how to climb from valley to mountain top. Indeed however, the wetting work W to overcome the resistance of TPCL moving along pillar wall during C–W transition should be considered to determine the necessary and sufficient condition of the conversion. For textured surfaces with high posts, this condition is:

$$E_{\mathrm{bC}} + W \leq 0. \tag{37}$$

But for surfaces with short posts, the condition according to sag mechanism is

$$h_x \geq H. \tag{38}$$

In this latter situation, depinning of the TPCL below a droplet is not necessary.

The W in Eq. (37) is just the work to wet the pillar side walls during the TPCL beneath a droplet depinning and moving towards the substrate of textures, which is expressed by

$$W = \pi r_{\mathrm{s}}^2 (r-1)\, \sigma_{\mathrm{LG}} |\cos\theta_{\mathrm{A}}|, \tag{39}$$

where θ_{A} is the advancing contact angle when the TPCL moves forward.[27,40,41]

Then equation (37) or (38) is the necessary and sufficient condition of C–W transition, and can be used to determine the wetting state of a droplet and the C–W transition on textured surfaces.

4.6. Comparison between measured C–W transition parameters and calculating results

There are two types of reported experiments to investigate droplets C–W transition on rough surfaces. One of them is to monitor the changes of contact angles of fixed volume droplets deposited on surfaces with different textured parameters. And the C–W transition could be reflected by the sudden change of contact angles. The second way is to identify the abrupt deviation of shape parameters of a droplet during its evaporation on a rough surface. The experimental results from literatures and the corresponding calculation results with this model are compared in Fig. 8 to Fig. 10.

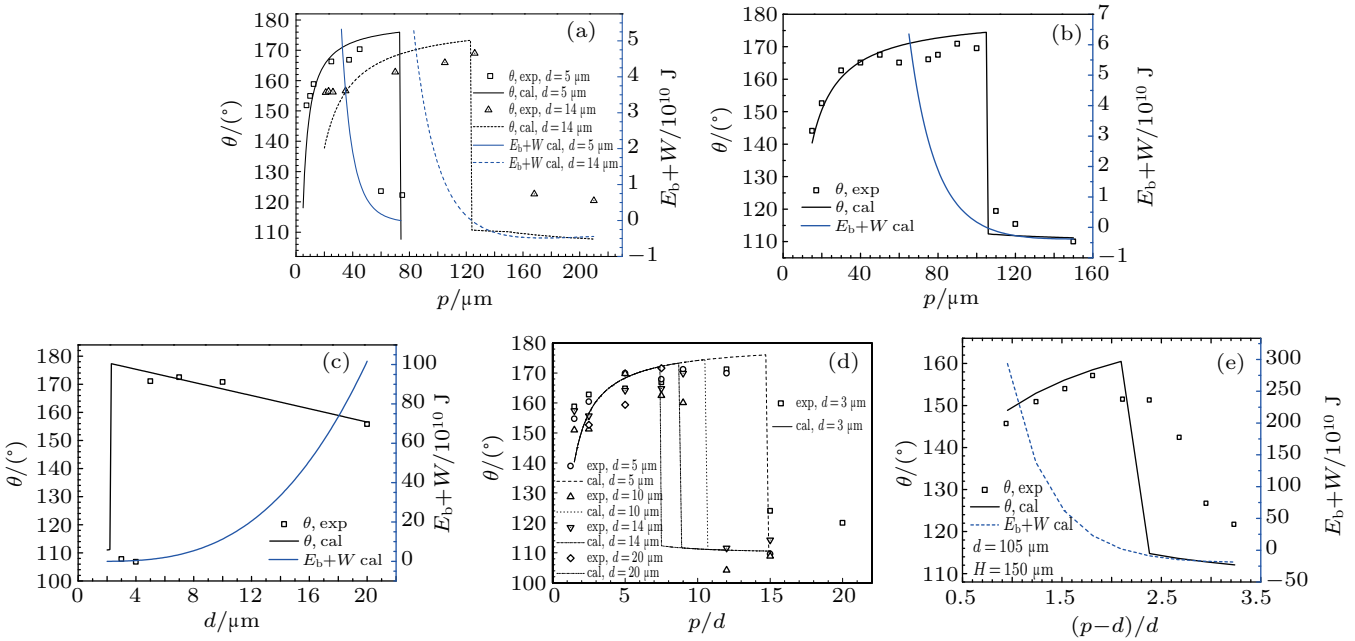


Fig. 8. (color online) Changes of contact angle and IFE barrier E_{b} plus wetting work of sessile droplets before and after C–W translation on different textured surfaces. (a) experimental data originate from literature,[35] $H = 10$ μm when $d = 5$ μm, $H = 30$ μm when $d = 14$ μm; $V = 5$ μL, $\theta_{\mathrm{I}} = 109°$, $\theta_{\mathrm{A}} = 109°$; (b)–(d): experimental data originate from literature,[25] $V = 3$ μL, $\theta_{\mathrm{I}} = 110°$, $\theta_{\mathrm{A}} = 116°$, (b) $d = 10$ μm, $H = 40$ μm, (c) $p = 50$ μm, $H = 20$ μm, (d) $H = 2 \times d$; (e) experimental data originate from literature,[16] $V = 4.3$ μL, $\theta_{\mathrm{I}} = 107.5°$, $\theta_{\mathrm{A}} = 107.5°$.

As shown in Fig. 8, the contact angles of sessile droplets on different rough surfaces decline abruptly when C–W transition takes place. The model calculations are agreed well in general with the experimental results.[16,25,35] It can be seen from Figs. 8(a), 8(b), 8(d), and 8(e) that the enlargement of pillar pitch ultimately results in the droplet collapse. And it can be found from Fig. 8(c) that droplets simply appear in Cassie state as pillar diameter increases, but Wenzel droplets normally emerge on surfaces if the diameter of posts is small.

It is commonly considered that the C–W transition is limited by IFE energy barrier.[5,19,25,28,43,44] Once this energy barrier diminishes to zero, the C–W transition should take place.[7] However, the droplet C–W transition usually dose not happen even when the energy barrier is zero, but regularly takes place when energy barrier is evidently lower than zero.[25] The main reason for this is that energy barrier is a state function, which merely depends on the IFE difference of droplet between two states.[25] But the C–W transition on the

other hand relies on the process path, namely it is related to the process of TPCL moving along structural side walls.[44] Therefore, it is essential to consider not only the energy barrier but also the process work so that the C–W transition can be appropriately determined. The necessary and sufficient condition of C–W transition we developed in Eq. (36) involves not only energy barrier but also the wetting work W. And this criterion was used to determine the C–W transition in Figs. 8(a)–8(c), and 8(e), i.e., the sudden decrease of contact angles corresponds to energy barrier plus wetting work becoming zero. And the calculated C–W transition with this criterion is in good agreement with experiments.

While a Cassie state droplet evaporates on a rough surface, the energy barrier plus work declines continuously as the drop size reduces. As a result, the droplet will change into Wenzel state at a certain time when the energy barrier plus work becomes zero. It can be seen from Fig. 9 that the base area of the evaporating droplet suddenly enlarges apparently when the C–W transition takes place. And the conversion point calculated with this model fits the measured result[7] very well.

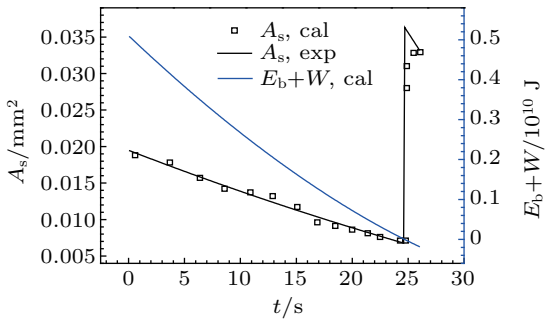


Fig. 9. (color online) Changes of base area and IFE barrier E_b plus wetting work of a droplet before and after its C–W translation during evaporation. Experimental data originate from literature.[7] $d = 3$ μm, $p = 20$ μm, $H = 4.8$ μm,, $\theta_A = 116°$. Note: the droplet volume required in model calculation was solved by using the measured droplet base area and receding contact angle.

Finally as shown in Fig. 10, the critical scale of an evaporating droplet when the C–W transition happens is clearly relative to pillar pitch p. When p is small, no C–W transition takes place for all scales of droplets during evaporation as contact angles do not reduce noticeably. But if p is great enough, the C–W transition will occur when the droplet scale decreases to a critical value, at which moment the contact angle of droplet declines abruptly and the droplet radius rises visibly. Generally, the calculations are in agreement with the measured results[34] except for the exact transition points where there is deviation between the calculation and the measurement. For example, the calculated critical radius of droplet when C–W transition happens is smaller than the measured value in the case of $d = 5$ μm (Fig. 10(a)), but the calculated critical radius is larger than the experimental value in the case of $d = 14$ μm (Fig. 10(b)). In view of the complexity of droplet C–W transition in evaporation process, the deviation between the calculation and the experiment for the C–W transition point is acceptable. Therefore the model is reliable to be used to determine droplet C–W transition because the calculations overall fit experimental results well.

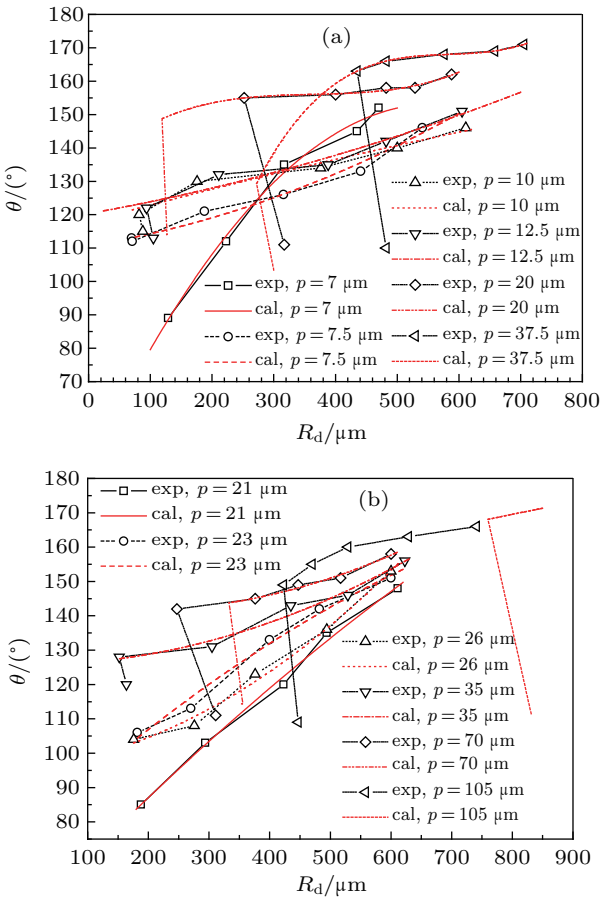


Fig. 10. (color online) Changes of contact angles before and after C–W transition of droplets during evaporation. Experimental data originate from literature,[35] $\theta_I = 109°$, $\theta_A = 109°$. (a) $d = 5$ μm, $H = 10$ μm; (b) $d = 14$ μm, $H = 30$ μm. Note: the droplet volume required in model calculation was solved by using the measured droplet radius and contact angle.

4.7. Line tension effect during the wetting transition

Line tension[51] is the free energy on unit TPCL. And the free energy of a droplet induced by line tension is the product of line tension and the total length of the TPCL at the bottom of the droplet. However, the IFE mentioned above is only limited to the free energy resulting from interfacial tension, which equals to the product of surface energy and the relative phase-contacted area. When a composite droplet sits on the solid surface with nanostructures the length value of the TPCL beneath the drop may be much larger than the value of contact area. Therefore, even though the line tension is usually obviously smaller than surface tension or surface free energy, the free energy induced by line tension still cannot be ignored.

In this model, the line tension induced free energy is not included. However, the calculation of energy barrier during C–W transition is not influenced since only the cylindrical

micro/nanostructure is considered. Consequently, the TPCL length of the droplet bottom is constant during the C–W transition, and the free energy induced by line tension is also unchanged. Therefore the energy barrier of C–W transition (Eq. (27) or Eq. (31)) will be the same no matter considering the free energy caused by line tension or not since the two terms on the right side of Eq. (27) both have the same free energy induced by line tension. However, if the nanostructure is in other shapes, e.g. cone or sphere, the present Eq. (27) or Eq. (31) will bring error because the free energy induced by line tension constantly changes during the C–W transition. In these latter cases, line tension induced free energy must be considered.

4.8. Consistency of the C–W transition analysis with free energy method and force balance

Both free energy and force balance methods can be used to analyse the C–W transition. We had applied the force analysis method[45] to develop a physical and mathematical model for the process judgement of the C–W transition. In that study, the interface free energy gradient was proposed as the driving force of C–W spontaneous transition. And the wetting force or capillary force on the TPCL on a hydrophobic surface was taken as the resistance preventing the TPCL depinning. Compared with the two calculation results of the force analysis and the present free energy method, they are almost the same. Therefore, the two methods are consistent with each other to analyze the C–W transition.

5. Conclusions

The liquid–air interface beneath a composite droplet in metastable state is either flat or curved on textured surfaces depending on the pitches between posts. The interface is in a plane shape when the pitches are relatively small, but in a curved mensicus when the pitches are comparatively large. The angle between the interface and pillar wall is the same as the supplementary angle of intrinsic contact angle. But the apparent contact angle and base radius of droplet are almost equal to the calculation according to Cassie–Baxter equation. The necessary and sufficient condition of C–W transition is the energy barrier plus wetting work of pillar walls beneath a droplet less than zero for textured surfaces with high posts, or the curved depth of meniscus greater than or equal to pillar height for structural surfaces with short posts.

References

[1] Werner O, Wågberg L and Lindström T 2005 *Langmuir* **21** 1223
[2] Li W and Amirfazli A 2007 *Adv. Colloid Interface* **132** 51
[3] Bahadur V and Garimella S V 2007 *Langmuir* **23** 4918
[4] Extr, C W 2002 *Langmuir* **18** 7991
[5] Kusumaatmaja H, Blow M L, Dupuis A and Yeomans J M 2008 *Europhys. Lett.* **81** 36003
[6] Extr, C W 2004 *Langmuir* **20** 5013
[7] Reyssat M, Yeomans J M and Quéré D 2008 *Europhys. Lett.* **81** 26006
[8] Gross M, Varnik F, Raabe D and Steinbach I 2010 *Phys. Rev. E* **81** 051606
[9] Papadopoulos P, Mammen L, Deng X, Vollmer D and Butt H J 2013 *P. Natl. Acad. Sci. USA* **110** 3254
[10] Rykaczewski K, Landin T, Walker M L, Scott J H J and Varanasi K K 2012 *ACS Nano* **6** 9326
[11] Rathgen H and Mugele F 2010 *Faraday Discuss.* **146** 49
[12] Lv P, Xue Y, Shi Y, Lin H and Duan H 2014 *Phys. Rev. Lett.* **112** 196101
[13] Oh J M, Manukyan G, Van den Ende D and Mugele F 2011 *Europhys. Lett.* **93** 56001
[14] Manukyan G, Oh J M, Van Den Ende D, Lammertink R, Mugele F 2011 *Phys. Rev. Lett.* **106** 014501
[15] Emami B, Tafreshi H V, Gad-el-Hak M and Tepper G 2011 *Appl. Phys. Lett.* **98** 203106
[16] Lee J B, Gwon H R, Lee S H and Cho M 2010 *Mater. Trans.* **51** 1709
[17] Xiu Y, Zhu L, Hess D W and Wong C 2007 *Nano Lett.* **7** 3388
[18] Liu B and Lange F F 2006 *J. Colloid Interf. Sci.* **298** 899
[19] David R and Neumann A W 2013 *Colloid. Surf. A* **425** 51
[20] Ensikat H J, Schulte A J, Koch K and Barthlott W 2009 *Langmuir* **25** 13077
[21] Bormashenko E, Pogreb R, Stein T, Whyman G, Erlich M, Musin A, Machavariani V and Aurbach D 2008 *Phys. Chem. Chem. Phys.* **10** 4056
[22] Im M, Im H, Lee J H, Yoon J B and Choi Y K 2010 *Langmuir* **26** 17389
[23] Shahraz A, Borhan A and Fichthorn K A 2012 *Langmuir* **28** 14227
[24] Moradi S, Englezos P and Hatzikiriakos S G 2013 *Colloid Polym. Sci.* **291** 317
[25] Barbieri L, Wagner E and Hoffmann P 2007 *Langmuir* **23** 1723
[26] Xue Y, Chu S, Lv P and Duan H 2012 *Langmuir* **28** 9440
[27] Quéré D 2008 *Annu. Rev. Mater. Res.* **38** 71
[28] Whyman G and Bormashenko E 2012 *J. Adhes. Sci. Technol.* **26** 207
[29] Xue Y, Lv P, Liu Y, Shi Y, Lin H and Duan H 2015 *Phys. Fluids* **27** 092003
[30] Bormashenko E 2010 *Philos. T. Roy. Soc. London A* **368** 4695
[31] Koishi T, Yasuoka K, Fujikawa S, Ebisuzaki T and Zeng X C 2009 *P. Natl. Acad. Sci. USA* **106** 8435
[32] Zheng Q S, Yu Y and Zhao Z H 2005 *Langmuir* **21** 12207
[33] Xue Y, Lv P, Lin H and Duan H 2016 *Appl. Mech. Rev.* **68** 030803
[34] Migliaccio C P and Garimella S V 2012 *Nanosc. Microsc. Therm.* **16** 154
[35] Jung Y and Bhushan B 2008 *J. Microsc-Oxford* **229** 127
[36] Tsai P, Lammertink R G H, Wessling M and Lohse D 2010 *Phys. Rev. Lett.* **104** 116102
[37] Lafuma A and Quéré D 2003 *Nat. Mater.* **2** 457
[38] Patankar N A 2010 *Langmuir* **26** 8941
[39] Patankar N A 2004 *Langmuir* **20** 7097
[40] Checco A, Ocko B M, Rahman A, Black C T, Tasinkevych M, Giacomello A and Dietrich S 2014 *Phys. Rev. Lett.* **112** 216101
[41] Kwon H M, Paxson A T, Varanasi K K and Patankar N A 2011 *Phys. Rev. Lett.* **106** 036102
[42] Marengo M, Antonini C, Roisman I V and Tropea C 2011 *Curr. Opin. Colloid .* **16** 292
[43] Whyman G and Bormashenko E 2011 *Langmuir* **27** 8171
[44] Bormashenko E, Musin A, Whyman G and Zinigrad M 2012 *Langmuir* **28** 3460
[45] Liu T Q, Li Y J, Li X Q and Sun W 2015 *Chin. Phys. B* **24** 116801
[46] Boreyko J B, Baker C H, Poley C R and Chen C H 2011 *Langmuir* **27** 7502
[47] Susarrey-Arce A, Marin A G, Nair H, Lefferts L, Gardeniers J, Lohse D and Van Hous A 2012 *Soft Matter* **8** 9765
[48] He Y, Jiang C, Wang S, Yin H and Yuan W 2013 *Appl. Surf. Sci.* **285** 682
[49] Luo C, Xiang M and Heng X 2012 *Langmuir* **28** 9554
[50] Luo C, Xiang M 2012 *Langmuir* **28** 13636
[51] Ma X H and Zhang Y 2003 *J. Basic Sci. Eng.* **12** 268 (in Chinese)